Nuclear Engineering and Technology 53 (2021) 3286–3297

Contents lists available at ScienceDirect

Nuclear Engineering and Technology

journal homepage: www.elsevier.com/locate/net

Original Article

A mechanistic analysis of H_2O and CO_2 diluent effect on hydrogen flammability limit considering flame extinction mechanism

Joongoo Jeon [a], Yeon Soo Kim [a], Hoichul Jung [a], Sung Joong Kim [a, b, *]

[a] Department of Nuclear Engineering, Hanyang University, 222 Wangsimni-ro, Seongdong-gu, Seoul, 04763, Republic of Korea
[b] Institute of Nano Science & Technology, Hanyang University, 222 Wangsimni-ro, Seongdong-gu, Seoul, 04763, Republic of Korea

ARTICLE INFO

Article history:
Received 12 October 2020
Received in revised form
9 April 2021
Accepted 5 May 2021
Available online 20 May 2021

Keywords:
Flammability limit
Radiating gas
Indirect radiation
Extinction mechanism
Hydrogen safety

ABSTRACT

The released hydrogen can be ignited even with weak ignition sources. This emphasizes the importance of the hydrogen flammability evaluation to prevent catastrophic failure in hydrogen related facilities including a nuclear power plant. Historically numerous attempts have been made to determine the flammability limit of hydrogen mixtures including several diluents. However, no analytical model has been developed to accurately predict the limit concentration for mixtures containing radiating gases. In this study, the effect of H_2O and CO_2 on flammability limit was investigated through a numerical simulation of lean limit hydrogen flames. The previous flammability limit model was improved based on the mechanistic investigation, with which the amount of indirect radiation heat loss could be estimated by the optically thin approximation. As a result, the sharp increase in limit concentration by H_2O could be explained by high thermal diffusivity and radiation rate. Despite the high radiation rate, however, CO_2 with the lower thermal diffusivity than the threshold cannot produce a noticeable increase in heat loss and ultimately limit concentration. We concluded that the proposed mechanistic analysis successfully explained the experimental results even including radiating gases. The accuracy of the improved model was verified through several flammability experiments for H_2-air-diluent.

1. Introduction

During a severe accident in a nuclear power plant (NPP), hydrogen is produced by the oxidation of rector core and get distributed in the containment [1,2]. If the local hydrogen concentration exceeds the lower flammability limit (LFL), flame acceleration and detonation can occur depending on the mixture and geometric conditions, and their potential risk should be evaluated based on rigorous regulatory standards [3]. The LFL is the minimum fuel concentration required for a flame to continuously propagate by ignition. Thus, it is of paramount importance to clarify the LFL of hydrogen mixtures as the first criterion for the hydrogen risk assessment of NPPs [4]. In addition to the nuclear industry, the knowledge concerning the flammability limit is essential to ascertain the safety of combustion-related events during production, storage, and transportation of hydrogen fuel [5]. As shown in Fig. 1, the trend of LFL varies completely depending on the diluent type. It primarily depends on the initial temperature as well as diluent type and concentration. Although the LFL of hydrogen mixtures has been determined through many experimental studies, it is infeasible to investigate all possible mixtures in various accident scenarios. Experimental results are especially deficient when radiating gases are included as diluent [6].

Many historical attempts have been made to explain the limit concentration at which combustion occurs via thermal analysis [7–11]. These attempts can be divided into two categories: macroscopic and microscopic methods [6]. The macroscopic method analyzes the overall energy balance with combustion heat, from which useful insight by the properties of burned gas can be acquired on the macro scale [9,12,13]. One of the most notable findings of this method was to utilize the concept of calculated adiabatic flame temperature (CAFT) by Vidal et al. [9]. They insisted that the parameter of adiabatic flame temperature is a powerful tool for estimating the LFL of hydrocarbon fuels. In contrast, the microscopic method calculates the multi-step chemical reactions and detailed diffusion effects of the millimeter unit in milliseconds to simulate flame propagation [14–16]. However, it has not yet been reported that the accuracy is maintained under various

* Corresponding author. Department of Nuclear Engineering, Hanyang University, 222 Wangsimni-ro, Seongdong-gu, Seoul, 04763, Republic of Korea.
E-mail address: sungjkim@hanyang.ac.kr (S.J. Kim).

https://doi.org/10.1016/j.net.2021.05.004

Nomenclature

a	Planck's mean absorption coefficient (m/atm)
C	Molar concentration (mol/m^3)
c_p	Heat capacity at constant pressure (J/kg·K)
$\tilde{D}$	Modified diffusion coefficient accounting for thermal diffusion (m^2/s)
ΔH_f^0	Standard formation enthalpy (J/mol)
k	Thermal conductivity (W/m·K)
$\tilde{Le}_{H_2}$	Effective hydrogen Lewis number
M	Molecular mass (kg)
n	*Converted* mole number $n_i = n_i / \sum_{reactants} n_i$ (mole)
p	Partial pressure (atm)
Q_{rad}	Total radiative heat loss in mole unit (kJ/mol)
$Q_{rad,1}$	Indirect radiation heat loss in mole unit (kJ/mol)
q_{rad}	Total radiative heat loss per unit area (W/m^2)
$q_{rad,1}$	Indirect radiation heat loss per unit area (W/m^2)
R	Radiative volumetric heat loss (W/m^3)
r	Radius of flame ball (m)
S_u	Laminar flame speed (m/s)
T_u	Unburned mixture temperature (K)
T_0	Ambient temperature (K)
T_{ref}	Reference temperature (K)
T_{peak}	Peak flame temperature (K)
T_{CAFT}	Calculated adiabatic flame temperature (K)
T_{CNAFT}	Calculated non-adiabatic flame temperature (K)
X	Mole fraction
Y	Mass fraction
$\tilde{Y}$	Modified mass fraction

Greek letters

α	Thermal diffusivity (m^2/s)
π	CNAFT coefficient
ρ	Density (kg/m^3)
σ	Stephan-Boltzmann constant (W/m^2·K^4)

diluent conditions because the uncertainties related to the chemical kinetics or diffusion coefficients may distort the simulation results [17]. The expected increase in computing costs to alleviate these uncertainties is particularly pronounced when the calculation of thermal radiation is performed in a very fine grid. Therefore, most severe accident analysis codes such as MAAP developed by Fauske and Associates Inc. and MELCOR by Sandia National Laboratories still rely on experimental results [18].

Recently, a calculated non-adiabatic flame temperature (CNAFT) model was developed to predict the hydrogen flammability limit by considering the heat loss mechanism [19]. The proposed model analyzed the physics of flame propagation in a non-adiabatic condition by focusing on heat loss mechanisms during upward propagation. They suggested that that thermal radiation ultimately determined the total heat loss from the reaction zone and its amount could be estimated using the CNAFT coefficient. The model showed good agreement with the LFL values measured experimentally for various diluent conditions. The bar graph of helium in Fig. 1 shows that as the CNAFT coefficient increased, the LFL concentration also increased. For the flame to propagate, increasing heat loss with helium concentration necessitates the higher hydrogen concentration. In contrast, the increase in argon concentration showed the opposite effects. However, it was confirmed that the accuracy of the CNAFT model significantly decreased for H_2-air-steam mixtures, which include radiating species of steam. In severe accident analysis, the prediction of hydrogen combustion risk is generally focused on the H_2-air-steam mixtures in most scenarios because the large amounts of coolant are released from the reactor coolant system. The assumption of constant radiation rate applied in the previous model seems no longer valid because steam is classified as a radiating gas. It was noted that the effect on the flammability limit of carbon dioxide, another radiating species, also had yet to be thoroughly analyzed. The carbon dioxide can be produced by the molten corium-concrete interaction during an ex-vessel phase [20].

In addition, a preceded observation of the nature of hydrogen flame extinction is essential to identify the valid of the one-dimensional thermal analysis. In other words, the Lewis number effect on the actual flame extinction mechanism and mechanistic LFL prediction needs to be investigated. Recent experimental and numerical studies with stabilized flame method observed that the upward propagating lean hydrogen flame can have a few shapes as it approaches the limit concentration [21,22]. The transition of flame shape before final extinction was identified for hydrogen flame whereas the extinction of methane flame proceeds directly from the bubble-like flame. It seems that the different extinction process of the lean hydrogen flame is deeply related to the need for

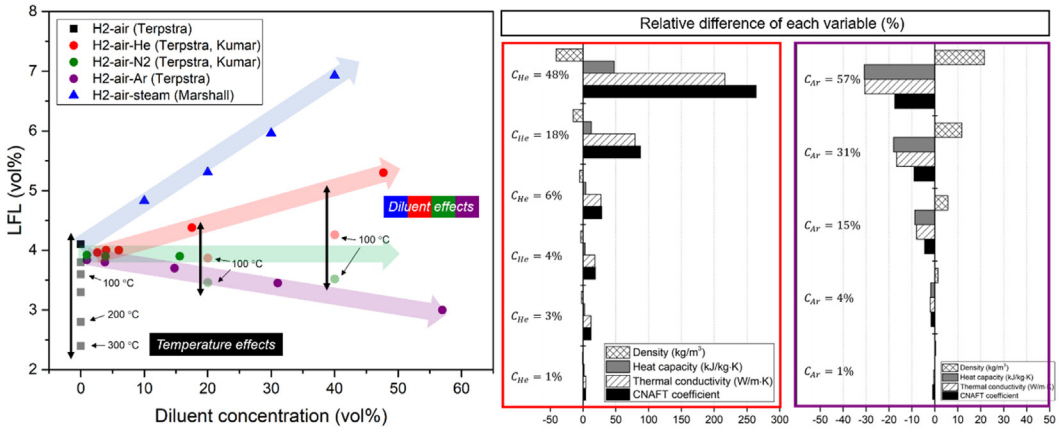

Fig. 1. Variation of lower flammability limit by temperature and diluent effects. The bar graphs show the increase (H_2-air-He) and decrease (H_2-air-Ar) of the CNAFT coefficient by diluent concentration.

a non-adiabatic thermal model. Considering the foregoing discussion on the general background and technical limitations of the CNAFT model developed previously, the objectives of this study can be summarized as follows:

1) To numerically investigate the lean limit hydrogen flames to observe the extinction process
2) To clarify the reason for the reduced accuracy of the CNAFT model for radiating gas and overcome this discrepancy by thermal modeling.

The improved accuracy of the CNAFT model was verified by several flammability experiments because comparisons only to a single experiment may yield a biased confirmation on model reliability [23–25].

2. Extinction process of lean limit hydrogen flame

In this study, the lean hydrogen flames were numerically investigated with the Fluent 18.0 code which was a multi-purpose CFD code for industrial applications such as fluid and gas dynamics, heat transfer. By simulating hydrogen flames while lowering the hydrogen concentration, the flame extinction process for theoretical modeling can be understood. The Fluent-CHEMKIN solver was especially developed to analyze fluid dynamics with chemical combustion. Table 1 shows simulation conditions and models used in this study. The computational domain is an axisymmetric geometry with a height of 100 mm and a diameter of 25 mm as shown Fig. 2. This diameter is the same size with the study to observe the flame extinction of stretched methane flame [26]. The weighted-sum-of-gray-gas model can calculate the total radiative quantities for a small number of gray gases with discrete ordinate method [27,28].

The species transport model, which can calculate the mixing and transport of chemical species by solving conservation equation describing convection, diffusion and detailed chemical kinetics for each component species, was used for observing the flame structure. Recently, Zhou et al. suggested that the hydrogen flames can be stabilized as the flame blow-off limit in a downward inlet velocity corresponding to the measured upward propagating flame speed (stabilized flame method) [21]. This method allows to observe the flame characteristics as fuel concentration approaches the limit through the steady solver [21,22]. Since the flame propagation speed in the stable flame region for lean limit hydrogen mixtures was measured to be almost constant at 0.12 m/s, the inlet velocity was determined as that value [29]. In our sensitivity study, it was identified that the flame blown away from the computational domain if the inlet velocity was too larger than 0.12 m/s as previous studies suggested [21,22]. Conversely, too lower inlet velocity

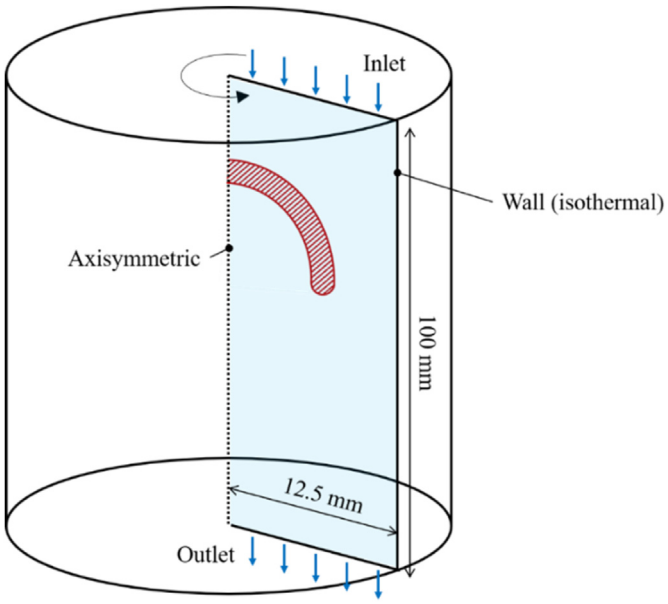

Fig. 2. Axisymmetric cylindrical domain and boundary conditions.

caused the flame flashback to the inlet boundary. Under the velocity close to 0.12 m/s the axial distances where the flame was formed were slightly different, but the stabilized flame showed near identical characteristics. The results, in which the stabilized flames were only observed around unified inlet velocity independent on mixture conditions, verified our simulation method.

Fig. 3 shows the observed flame shapes and flow patterns near the flame according to the hydrogen concentration. The color map displays the temperature based on each color scale. The dotted line depicts the reaction zone based on the OH radical field. Since most sub-kinetics to generate steam include OH radical as shown in Table 2, the structure of hydrogen flame has been analyzed by OH radical field [16,22]. The flow pattern of unburned gas is nearly identical with the calculated velocity field for upward propagation based on the coordinate system moving together with the flame [21]. In 6.0 vol%, the bubble-like flame with a long flame skirt was predicted as shown Fig. 3(a). The downward flow was observed for all regions before and after entering the reaction zone due to quite higher hydrogen concentration than limit concentration. The flame burning velocity of this mixture is enough to suppress the buoyancy-driven convection flow. The burning intensity was focused on the flame tip by the Lewis number effect (preferential diffusion effect) due to small Lewis number of lean hydrogen mixture($Le < 1$).

Table 1
Simulation conditions and models to analyze stabilized flame structure.

General	Type	Model
Geometry	Geometry	H: 100, R: 12.5 mm (axisymmetric)
	Mesh size	0.1×0.1 mm
	Total mesh	~ 125000
Solver	Solver	Fluent-CHEMKIN
	Time	Steady
	Viscous	Laminar model
	Species	Species Transport model
	Radiation	DO model with WSGGM
	Kinetics	San Diego mechanism
Boundary conditions	Inlet	Velocity inlet
	Outlet	Pressure outlet
	Wall	Non-slip, isothermal
	Ignition temperature	1200 K

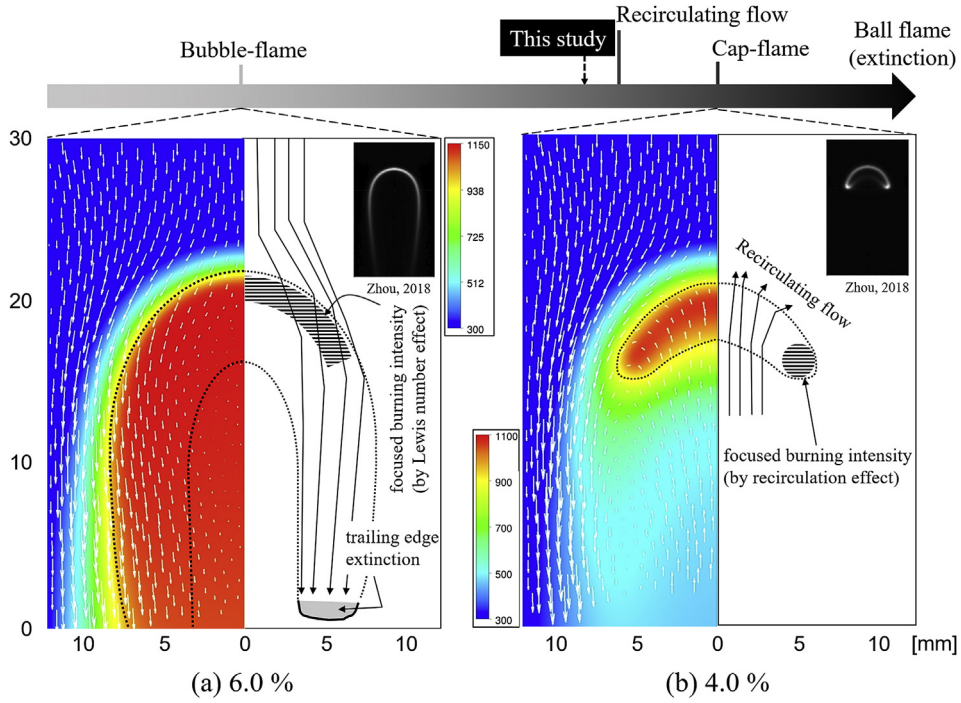

Fig. 3. Variation of flame shape and flow pattern with decreasing hydrogen concentration. The transition from the bubble-like flame to the cap-like flame occurred due to the primary extinction of the trailing edge.

Table 2
20 reversible elementary reactions in San Diego mechanism for hydrogen combustion [14].

Type	Reaction
Shuffle reactions	$H + O_2 \leftrightarrow OH + O$ $H_2 + O \leftrightarrow OH + H$ $H_2 + OH \leftrightarrow H_2O + H$ $H_2O + O \leftrightarrow OH + OH$
Hydroperoxyl reactions	$H + O_2 + M \leftrightarrow HO_2 + M$ $HO_2 + H \leftrightarrow OH + OH$ $HO_2 + H \leftrightarrow H_2 + O_2$ $HO_2 + H \leftrightarrow H_2O + O$ $HO_2 + O \leftrightarrow OH + O_2$ $HO_2 + OH \leftrightarrow H_2O + O_2$
Radical-radical recombination reactions	$H + OH + M \leftrightarrow H_2O + M$ $H + H + M \leftrightarrow H_2 + M$ $O + O + M \leftrightarrow O_2 + M$ $H + O + M \leftrightarrow OH + M$
Hydrogen peroxide reactions	$OH + OH + M \leftrightarrow H_2O_2 + M$ $HO_2 + HO_2 \leftrightarrow H_2O_2 + O_2$ $H_2O_2 + H \leftrightarrow HO_2 + H_2$ $H_2O_2 + H \leftrightarrow H_2O + OH$ $H_2O_2 + OH \leftrightarrow H_2O + HO_2$ $H_2O_2 + O \leftrightarrow HO_2 + OH$

The Lewis number is a dimensionless number defined as the ratio of thermal diffusivity to mass diffusivity. The preferential diffusion effects were increases as the Lewis number becomes smaller than unity. For this reason, the length of flame skirt was gradually shortened instead of flame tip extinction as the hydrogen concentration decreased. The reason why the trailing edge disappears continuously seems that the elevated negative temperature gradient due to slow exit velocity at flame front. The trailing edge was defined as the end of the reaction zone in this study (Fig. 3). As suggested in many thermal theories, the conduction (indirect radiation) mechanism caused by the negative temperature gradient can account for the flame extinction [19,30–32].

In 4.5 vol% hydrogen flame, the noticeable decrease in flame skirt length was identified as shown in Fig. 3(b). As the length of flame skirt is shortened, the transition from the bubble-like flame to the cap-like flame occurs. During this extinction process, the recirculating flow was observed for the region below the reaction zone. It is of interest to note that the simulated flame-shaped transition process was also identical with the recent experimental results. Zhou et al. experimentally observed lean hydrogen flames with stabilized flame method [22]. The OH* chemiluminescence was recorded by an CCD camera to capture hydrogen flames. Similar to our simulation, the flame characteristics were investigated while decreasing the inlet hydrogen concentration ($\phi = 0.17$, 0.15, 0.13, 0.11). The length of flame skirt continued to decrease as the hydrogen concentration decreased and cap-like flames were captured from a certain concentration. They also identified the generation of the recirculating flow as hydrogen flame extinction occurred [22]. For comparison between our simulation results and captured real flame, the chemiluminescence images from similar geometry condition were included as shown in Fig. 3 [21].

Not only in the experiments of the stabilized flame method [21,22,33], but the transition from the bubble flame with long skirt to the cap flame were confirmed in freely propagating flame experiments (Table 3) [34,35]. In 25–50 mm standard tube, cap flames were identified for near lean limit mixtures containing hydrogen fuel as described in Ref. [34]. Recently, Volodin et al. captured the cap flame structure by the infrared camera and shadowgraphy photo. They suggested that the vortical flow, which bended and stretched the front surface, lead to the formation of an axisymmetric cap-flame in ultralean hydrogen flames. Even though a bubble flame was initially formed with a high ignition energy, the lean limit flame experienced the transition process to the cap shape through the energy balance between the combustion heat and heat loss. The prerequisite for the transition occurrence is the presence of the terrestrial gravity (normal gravity). Zhou et al. explained the main reason for this recirculation zone is due to the decrease of

Table 3
Recent experimental studies of the lean limit flames in terrestrial gravity conditions.

Year	Authors	Fuel type	Experimental method	Ref.
2010	Shoshin et al.	CH_4, H_2/CH_4	tube	[34]
2015	Hernandez-Perez et al.	H_2/CH_4	stabilized flame	[33]
2018	Zhou et al.	CH_4, H_2/CH_4, H_2	stabilized flame	[22]
2021	Volodin et al.	H_2	Chamber	[35]

burning velocity relative to the buoyancy-driven convection flow. We noted that the focused burning intensity region due to the Lewis number effect was also reversed as the direction of the fuel was reversed. It means that the intensity at the flame tip became relatively weaker. This reversal phenomenon of the intensity was analyzed in more detail in Ref. [32].

Shoshin et al. identified that the outflow rate of combustion products from the reaction zone was reduced at the methane flame tip in ultralean flames. For this reason, they concluded that the reason for the flame extinction was owing to the generated stagnation zone below the flame tip due to the elevated stretch rate [36]. However, we confirmed that the hydrogen flame extinction process is remarkably different with methane flame where extinction for upward propagating flame always started at the tip [37]. Since the flame stretch rate at the trailing edge is definitely lower than flame tip, it is difficult to understand this hydrogen extinction process by the stretch extinction theory [38]. We concluded that the generation of recirculating flow causing the weak burning intensity at the flame tip is a major branching point for hydrogen flame extinction. Because the stretch extinction effects can no longer be compensated by the Lewis number effect under recirculating flow, the hydrogen flame extinction occurs at a slightly lower concentration than for the cap flame generation. To reach the flame region generating recirculating flow, the length of flame skirt should be short enough by indirect radiation heat loss (primary extinction).

In this study, a thermal model for flammability limit was developed based on the extinction mechanism of the trailing edge. Since it is difficult to consider the negative flame speed by one-dimensional analysis, the mechanistic thermal modeling to predict the limit concentration was based on the regime immediately before the generation of the recirculation flow. Although hydrogen flames can be stabilized slightly below the concentration at which recirculation flow begins to occur, this approach enables universal theoretical model development.

3. Improved thermal model for LFL prediction

3.1. Analytical studies to confirm the limitations of the CAFT model

The previous studies remarked that peak temperature was proportional to the CAFT and therefore the LFL concentration reaching the threshold peak temperature was predicted by calculating the adiabatic temperature [6,8,9]. The CAFT frequently used variable in heat transfer analysis of premixed flame can be calculated as shown Eq. (1) [39,40]. To simplify the calculation, the moles of each gas were converted based on the total moles of reactants $\left(n_i = n_i / \sum_{reactants} n_i\right)$. If the initial temperature of unburned gas T_u is room temperature, the sensible heat term of reactants can be omitted. In addition to Vidal, many researchers have confirmed that the CAFT model showed reasonable accuracy in predicting the LFL in the hydrocarbon fuel including carbon monoxide [9,41].

$$\sum_{reactants} n_i\left[\Delta H^0_{f,i} + \bar{c}_{p,i}\left(T_u - T_{ref}\right)\right] - \sum_{products} n_i\left[\Delta H^0_{f,i} + \bar{c}_{p,i}\left(T_{CAFT} - T_{ref}\right)\right] = 0 \quad (1)$$

Although the physical background was discussed in detail in Refs. [8,9,19], a non-propagating spherical flame-ball analysis analytically confirming the limitation of the CAFT model was introduced in this study. For the stoichiometry of the global reaction $2H_2 + O_2 \rightarrow 2H_2O$, Eq. (2) shows the energy conservation equation, where r is the radius of the flame ball, k is the thermal conductivity, R is the volumetric radiation rate, and D is the mass diffusivity.

$$\frac{1}{r^2}\frac{d}{dr}\left(kr^2\frac{dT}{dr}\right) = R + \frac{\Delta H^0_{f,H_2O}}{r^2}\frac{d}{dr}\left(\frac{\rho\tilde{D}_{H_2}r^2}{M_{H_2}}\frac{d\tilde{Y}_{H_2}}{dr}\right) \quad (2)$$

If the radiation heat loss is neglected, the temperature at the reaction layer can be estimated by integrating Eq. (2) twice assuming constant $\rho\tilde{D}_{H_2}/k$ as shown Eq. (3).

$$T - T_u = \frac{\rho\tilde{D}_{H_2}}{k}\frac{\left(-\Delta H^0_{f,H_2O}\right)}{M_{H_2}}\left(Y_{H_2u} - \tilde{Y}_{H_2}\right) \quad (3)$$

As a result, the peak temperature at the reaction layer ($\tilde{Y}_{H_2} \cong 0$) can be estimated by Eq. (4). For comparison with the adiabatic temperature in Eq. (1), mole fraction is used as the unit.

$$T_{peak} = T_u + \frac{\rho\tilde{D}_{H_2}}{k}\left(-\Delta H^0_{f,H_2O}\right)X_{H_2u} \quad (4)$$

The proportional relation between peak temperature and CAFT can be confirmed using Eq. (5). It means that the linear proportionality between two variables, which has been remarked by previous research, can also be asserted in the form of an equation. $\bar{c}^*_p$ is the average specific heat for all constituent mixtures, and $\widetilde{Le}_{H_2}$ is the effective Lewis number which is an intrinsic mixture property [14]. For hydrogen-air premixed combustion, the effective Lewis number near the lean flammability limit is close to 0.3 [14]. However, it should be noted that the linear equation was valid only if the thermal radiation effect was neglected.

$$\frac{T_{peak} - T_u}{T_{CAFT} - T_u} = \frac{\rho\bar{c}^*_p\tilde{D}_{H_2}}{k} = \frac{1}{\widetilde{Le}_{H_2}} \quad (5)$$

Recently, Jeon et al. investigated the validity of the CAFT model for hydrogen mixtures in nuclear reactor severe accident [19]. As the model suggested, the CAFT was nearly constant for various lean limit hydrogen mixtures at approximately 600 K. However, prediction discrepancy was pronounced, especially when the initial temperature or steam concentration was high, which is a typical condition for hydrogen risk analysis in severe accident conditions. This limitation was caused by the unrealistic assumption of adiabatic flame propagation. In reality, the hydrogen flames do not propagate under adiabatic conditions, and the length of flame skirt is continuously shortened by indirect radiation heat loss as described in *Section 2*. In other words, the effect of the neglected thermal radiation causes limitations of the CAFT model for hydrogen mixtures. This provides a rationale that the heat loss effect depending on the mixture conditions should be considered when predicting LFL.

3.2. Calculated non-adiabatic flame temperature model

A CNAFT model was developed to overcome the reduced accuracy of CAFT model associated with adiabatic assumption [6,19]. Fig. 4 shows a schematic diagram of each method, which analyzes flame physics to predict LFL, described in *Section 1*. The simplest LFL prediction method assuming an adiabatic flame is shown in Fig. 4(a), and the most complex method that requires a very fine mesh and numerical calculations of multi-step reactions on the micro scale is shown in Fig. 4(c). In contrast, as shown in Fig. 4(b), the CNAFT model includes the macroscopic heat loss mechanism shown in Eq. (6). Many historical studies suggested that the heat loss mechanisms from the reaction zone to the post-reaction zone play an important role in determining the peak temperature [12,36,42]. In other words, the heat loss mechanism ultimately affects the flammability limit of mixtures. As shown in Fig. 4(b) and Eq. (6), this model suggested that the peak temperature is proportional to the CNAFT and not to the adiabatic temperature. The purpose of this model is to reasonably estimate the actual heat loss while preserving the advantages (simplicity and no complex chemical kinetics) of the CAFT model [19].

$$\sum_{reactants} n_i\left[\Delta H^0_{f,i}+\bar{c}_{p,i}\left(T_i-T_{ref}\right)\right] - \sum_{products} n_i\left[\Delta H^0_{f,i}+\bar{c}_{p,i}\left(T_{CNAFT}-T_{ref}\right)\right]=Q_{rad,1} \tag{6}$$

In our previous study, it was confirmed that the total amount of the radiation heat loss from the flame to the atmosphere can be estimated by considering conduction $Q_{rad,1}$ solely [19,32]. The conduction mechanism transfers heat from the reaction zone to the post reaction zone, which is cooled via radiative heat loss. Because the negative temperature gradient near the end of the reaction zone results from thermal radiation, the mechanism was named indirect radiation $Q_{rad,1}$ in conventional classification [31]. The radiative heat loss rate from the reaction zone itself (direct radiation) can be calculated with integration of the space-averaged radiative volumetric heat loss. By our simulation results, it was confirmed that the total direct radiation heat release rate based on the maximum volumetric rate did not reach 5% of the total direct radiation rate based on the minimum temperature gradient [32]. This significantly small effect on the trailing edge extinction of thermal radiation itself even get smaller when the total heat release rate was precisely calculated through the surface and volume integration. The negligible magnitude of direct radiation for flame propagation has also been confirmed in other previous studies [43]. Turns stated that the negative temperature gradient caused by thermal radiation can account for the existence of the flammability limit [30].

The heat flux $q_{rad,1}$ can be calculated with a peak temperature gradient under the influence of radiative heat loss, as shown in Eq. (7) [19,31]. The equation consists of several variables determined by the mixture properties and more details were described in Ref. [19]. The density and specific heat are obtained based on the unburned gas temperature. Changes in the specific heat are assumed to be negligible [31].

$$q_{rad,1}=k_f\frac{R}{\rho_u c_p S_u} \tag{7}$$

Although this one-dimensional thermal analysis is difficult to predict the temperature of the strongly stretched flame tip region, the primary extinction of hydrogen flame occurs at the nearly unstretched trailing edge as described in *Section 3*. Therefore, it was attempted to estimate the heat loss amount at the trailing edge by this one-dimensional thermal analysis. Since the stagnation zone was formed in the central region, we can estimate the indirect radiation rate at the trailing edge by assuming $\rho_u S_u = (\rho_b S_b)_{trailing\ edge}$. To calculate the flame temperature by energy balance in mole units, thermal diffusivity α divided by the molar concentration C was defined as the CNAFT coefficient π, as shown in Eq. (8). In addition, the volumetric radiation rate was treated as constant for lean limit hydrogen mixtures [19] because the lean limit hydrogen flame has a threshold peak temperature [8,9]. Although the experimental results for very lean mixture are very limited, the results from Koroll et al. show that the laminar flame speed also converges as the lean limit approaches. Recent studies also emphasized that the laminar flame speed can be used to characterize flammability limits [44]. We assumed that this approach is feasible at the trailing edge during the cap-like flame end period. Consequently, $Q_{rad,1}$ can be predicted using a linear function of the CNAFT coefficient (Eq. (8)).

In our previous study, the hydrogen mixtures were divided into two groups to confirm that the coefficient can represent the magnitude of heat loss [19]. The first group includes the mixtures having lower coefficients than the ambient air, and the second group has the mixtures with higher coefficients. While all mixtures in the first group showed a relative error less than 6%, the second group showed the maximum relative error close to 40%. These results confirmed that the limitation of the CAFT model originates from the adiabatic assumption [6,19]. This quantitative evaluation is a crucial evidence to confirm that the conducted one-

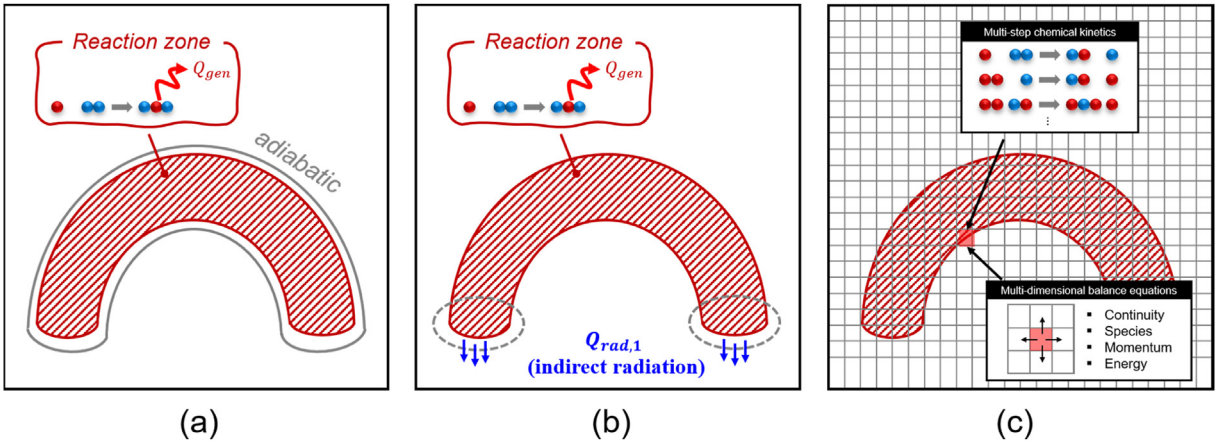

Fig. 4. Comparison of methods for predicting LFL. (a) CAFT model, (b) CNAFT model, and (c) microscopic method with numerical calculation.

dimensional thermal analysis can clarify the limitations of the previous adiabatic model.

The linearity derived mechanistically in Eq. (8) as well as the suitability of the coefficient were validated using the experimental results by Terpstra and Marshall in Table 4. Fig. 5 shows the difference of volumetric heat loss for each mixture based on their initial mole number before the reaction. The difference was inversely calculated using Eq. (6) based on the H_2-air mixture at room temperature (T_{CNAFT} = 610 K), as noted in our previous study [19]. The difference in the CNAFT coefficient was also calculated based on the reference mixture. As a result, a proportional relationship between the two variables was confirmed, and Eq. (9) was determined by the least-square analysis with an R^2 value of 0.98. The strong linearity of two variables emphasized the validity of constant volumetric radiation rate assumption except for H_2-air-steam mixtures. The H_2-air-CO_2 mixtures also contain a radiating gas, CO_2, but there is no difference in heat loss amount from the reference mixture. It was noted that $\pi - \pi_{ref} \cong 0$ for H_2-air-CO_2 mixtures regardless of the CO_2 concentration. It seems that the adiabatic condition was approached regardless of the diluent type even radiating gas, below the threshold value π_{ref} of the CNAFT coefficient.

$$Q_{rad,1} \sim k_f \frac{R}{\rho_u c_p S_u C} \sim \frac{\alpha}{C}\frac{R}{S_u} \sim \frac{\alpha}{C} \tag{8}$$

$$Q_{rad,1}(\pi) = 0.207\left(\pi - \pi_{ref}\right),\ \pi = \frac{\alpha}{C}\left[10^3 \cdot cm^5 \,/\, mol \cdot s\right] \tag{9}$$

Fig. 6 shows the reliability of the model for hydrogen mixtures through comparison with the various experimental results shown in Table 4 [23–25]. The dark symbols represent a mixture whose initial temperature is room temperature, except for steam. The hydrogen concentration where the CNAFT reached 610 K using Eqs. (6) and (9) is the predicted LFL value. Comparison with a single experiment can hinder reasonable confirmation of model reliability because various researchers focus on certain mixture conditions of their interest. For example, Terpstra's experimental matrix was constructed by various diluents including CO_2 [23], and Kumar included diluted hydrogen mixtures at elevated initial temperatures in the test matrix [24]. Marshall measured the flammability limit of hydrogen mixtures containing steam (FITS experiments) [25]. The reasonable accuracy of the model was confirmed even for H_2-air mixtures up to 300 °C. The reason why the linear relation between the CNAFT coefficient and radiative heat loss could not be identified for the H_2-air-steam mixture can be explained by the characteristics of the radiating gas. For hydrogen mixtures, where radiating gas are not included as the diluent, the volumetric radiation rate R is insensitive to mixture conditions. The steam classified as the radiating gas can be produced during combustion even if there is no steam in the initial mixture. However, the difference in the initial hydrogen concentration between the limiting mixtures is small enough to assume a constant value as described in Fig. 5. On the other hand, when a sizable amount of steam is initially included in the mixture, the effect of steam should be considered, as detailed in *Section 3.3*.

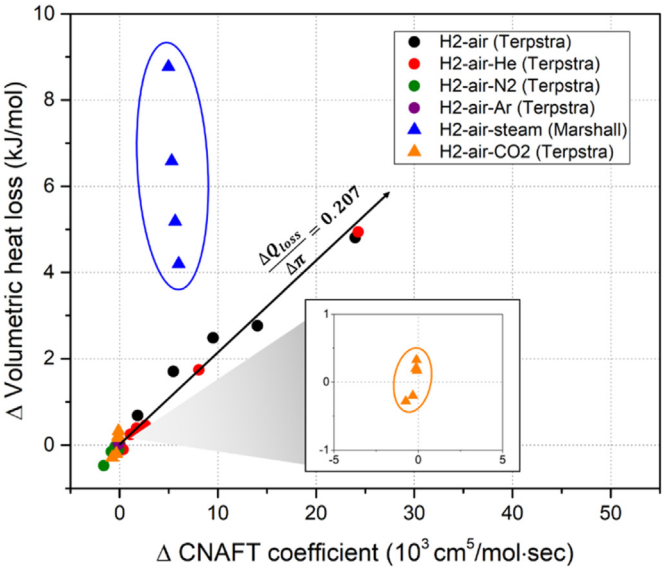

Fig. 5. Relationship between the CNAFT coefficient and volumetric heat loss for hydrogen mixtures. While steam causes larger heat loss than other diluents, a noticeable effect of CO_2 was not identified.

3.3. Thermal radiation effects of steam

Fig. 7 shows the amount of volumetric heat loss according to initial steam concentration based on the results from FITS experiments. The heat loss amount was calculated with the reference CNAFT value of 610 K. It was observed that the amount increased with increasing steam concentration. However, Eq. (9) cannot predict this increase because the increase in steam concentration led to a slight decrease in the CNAFT coefficient, as shown in Fig. 7. This indicates that the coefficient alone cannot estimate $Q_{rad,1}$ in H_2-air-steam mixtures. In lean hydrogen mixtures, the thermal

Table 4
CNAFT for various limiting mixtures.

Researcher	Mixture	T_i (°C)	Diluent (vol. %)	LFL (vol. %)	CNAFT (K)
Terpstra [23]	H_2-air	20	0	3.9	611
	H_2-air	50	0	3.8	620
	H_2-air	100	0	3.6	629
	H_2-air	150	0	3.3	627
	H_2-air	200	0	2.8	605
	H_2-air	300	0	2.4	605
	H_2-air-He	20	0–50	3.8–5.3	604–613
	H_2-air-Ar	20	0–60	3.0–3.8	604–612
	H_2-air-N_2	20	0–20	~ 3.9	616–622
	H_2-air-CO_2	20	0–40	3.9–4.6	606–621
Kumar [24]	H_2-O_2-He	22	20–40	5.1–5.8	664–691
	H_2-O_2-He	100	20–40	3.9–4.3	523–578
	H_2-O_2-N_2	22	20–40	~ 4.0	609–613
	H_2-O_2-N_2	100	20–40	~ 3.5	615–622
Marshall [25]	H_2-air-steam	383	10–40	4.8–6.9	597–652

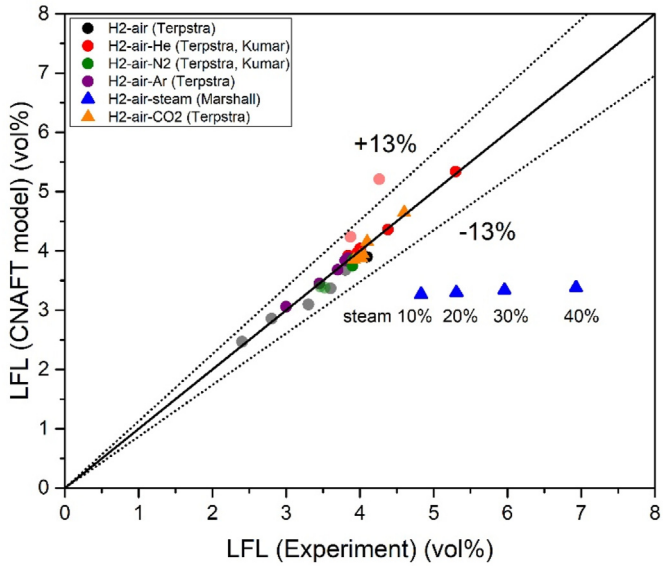

Fig. 6. Validation of the CNAFT model in various mixture conditions. The prediction accuracy was significantly reduced for H_2-air-steam mixtures.

radiation rate R in the flame front can be calculated with optically thin approximation [6,45], as shown in Eq. (10), where σ is the Stefan-Boltzmann constant, T_0 is the ambient temperature, p_{steam} is the partial pressure of steam, and a_{steam} is the Planck's mean absorption coefficient of steam. In constant peak flame temperature concept, the variation of the coefficient is negligible. Because the flame thickness at the lean limit flame was very small, the assumption of optically thin conditions was justified by referring to Hottel's charts [46]. In general, pure radiative loss from steam was included to estimate its amount because steam is considered to be the primary radiating species in hydrogen flame [42]. It is difficult to neglect changes in volumetric radiation rate in steam-diluted hydrogen mixtures, unlike other hydrogen mixtures. We confirmed that the radiation rate was expected to proportionally increase with steam partial pressure in this approximation method.

The experimentally observed increase of heat loss with steam concentration follows the conclusion of optically thin approximation. This logical connection is macroscopic evidence for the importance of indirect radiation for the trailing edge extinction.

$$R = 4\sigma\left(T_{peak}^4 - T_0^4\right)p_{steam}a_{steam} \tag{10}$$

The total amount of heat loss for a H_2-air-steam mixture can be estimated using Eq. (11) under isobaric conditions. The reference value $X_{steam,ref}$ is the steam mole fraction at the flame front in limit mixtures without dilution of steam. The flame front was defined as isoline of peak temperature in this study. Therefore, the amount of heat loss in a mixture containing steam can be estimated if the value of the steam mole fraction at the flame front $X_{steam,flame\ front}$ can be predicted. However, predicting the exact value of $X_{steam,flame\ front}$ according to each mixture is difficult. If complete combustion is possible at the flame front, heat loss can be calculated using the approximation shown in Eq. (12), which states that the sum of the initial hydrogen $X_{H_2,in}$ and steam mole fraction $X_{steam,in}$ is equal to $X_{steam,flame\ front}$. This assumption is difficult for whole combustion area, but possible at the flame front with very high temperature. As well as other previous studies [21], our simulation results also identified the complete combustion at the flame front of the trailing edge. The detailed observation for the temporal evolution of hydrogen and steam was described in Section 3.4. The reference steam mole fraction was defined as 0.05, which is the average of the LFL concentrations of mixtures without steam. This mean approximation is possible because the initial hydrogen concentrations between the limiting mixtures do not have appreciable scale differences as described in Fig. 5. Consequently, the heat loss amount was calculated using the sum of initial hydrogen and steam mole fraction. The steam effect term can be negligible when no steam is present in the initial mixture.

$$Q_{rad,1}(\pi) = 0.207\left(\pi - \pi_{ref}\right)\cdot\left(\frac{X_{steam,flame\ front}}{X_{steam,ref}}\right) \tag{11}$$

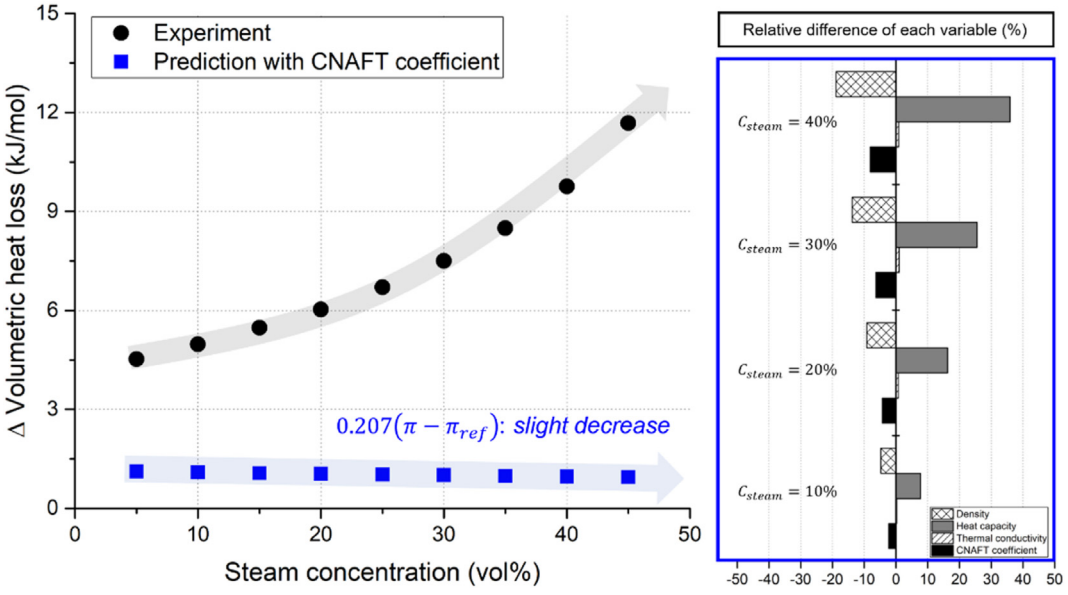

Fig. 7. Volumetric heat loss amount with steam concentration. The amount was calculated based on the FITS experiments and Eq. (9).

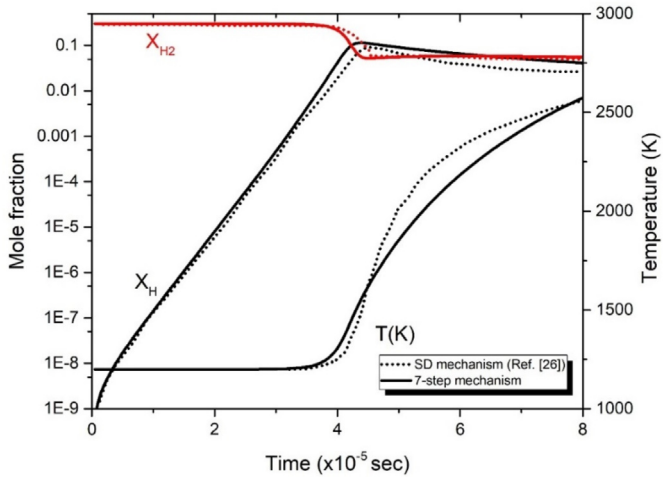

Fig. 8. Code validation for ignition of stoichiometric H_2-air mixture in a homogenous adiabatic reactor at constant atmospheric pressure and initial temperature T = 1200K.

$$\left(\frac{X_{steam,flame\ front}}{X_{steam,ref}}\right) \cong \left(\frac{X_{H_2,\ in} + X_{steam,\ in}}{X_{steam,ref}}\right) \tag{12}$$

3.4. The temporal evolution of gas species

To investigate the validity of the complete combustion assumption at flame front, an additional numerical simulation was conducted for homogenous H_2–air–steam mixtures. Although the overall complete combustion aspects at the flame front was observed, it was difficult to investigate the temporal evolution of hydrogen and steam concentration by the steady CFD simulation. On the other hand, computation of the ignition process between two semi-infinite spaces hydrogen and air allows to observe the temporal evolution [47]. In this study, the ignition processes of H_2–air–steam mixtures were computed in microsecond units by using the seven-step mechanism including three reversible shuffle reactions and the irreversible recombination. Fernandez-Gasliteo showed that, for ultralean hydrogen mixtures, the seven-step mechanism was sufficient to describe the progress of combustion [48]. The more detailed descriptions about the seven-step mechanism can be found in Ref. [48].

Fig. 8 shows the verification of our Matlab computation by using a typical time-dependent ignition history above crossover temperature for a stoichiometric H_2–air mixture with the San Diego mechanism obtained from Ref. [48]. The hydrogen concentration did not change initially but decreased rapidly at 40 μs. The reason for these delayed reactions is that the concentration of radicals, which can react with hydrogen, are significantly small initially. As production of radicals was amplified just before 40 μs, the hydrogen concentration rapidly decreased. It was identified that the seven-step chemical reaction provides sufficiently accurate results in the temporal evolution of the hydrogen mole fraction. Although the temperature change shows a slight difference, it is clear that this difference will be further reduced in lean conditions as noted by Fernandez-Gasliteo [48]. This code verification implies that the steam mole fraction at the flame front during propagation of hydrogen lean flame can be predicted through this simplified chemistry.

As the next step, ignition simulations for each H_2–air–steam mixture were performed with this verified seven-step reaction mechanism. The homogenous ignition at 1200 K, which is comparable with the peak flame temperature in our CFD results, was simulated to investigate the temporal evolution of hydrogen and steam mole fraction at the flame front for each limiting mixture as shown in Fig. 9. When the steam concentration is zero, the LFL is 4.1% and the mixture burns completely in about 150 μs. Rapid complete combustion was also observed in the other three cases with steam and the steam mole fraction in the burned gas was very close to the sum of initial hydrogen and steam mole fraction. Although the time to complete combustion slightly increased with the steam concentration, it was still significantly smaller than the flow timescale in the flame. The numerical results verify the assumption that the steam mole fraction during flame propagation can be substituted by the complete-combustion approach under lean conditions.

4. Results and discussion

Fig. 10 shows the accuracy of the derived optically thin approximation by comparing the experimental results. Unlike the approximated estimation, the experimental results show the rather non-linear increase in heat loss with steam concentration. Because the peak flame temperature bears a small difference depending on the mixture properties, this scale of error may occur. The error has a maximum value of 20% for mixtures with a steam concentration higher than 10%. Nevertheless, the discrepancy found in Fig. 5 was explained clearly through the thermal radiation theory, and the accuracy was improved significantly. This provides a rationale that the heat loss amount at the trailing edge can be estimated successfully by the developed thermal modeling.

By obtaining the thermal diffusivity of a mixture for which the LFL is not known experimentally, T_{CNAFT} can be calculated using Eq. (13). As mentioned earlier, the peak temperature during flame propagation is proportional to the CNAFT. Finally, the hydrogen concentration at which T_{CNAFT} reaches 610 K is determined as the LFL value. Noteworthly, the Lewis number effect on the local burning intensity at the trailing edge was investigated by introducing a constant factor, Ξ_{Le}. A Ξ_{Le} value smaller than 1 indicates that a needed hydrogen concentration for flammability was reduced due to the Lewis number effects. The change of Ξ_{Le} value according to the mixture type was investigated though the experimental results discussed in *Section 3.2*. As shown in Fig. 11, it was confirmed that the variation of Ξ_{Le} can be neglected in the developed thermal model.

$$\sum_{reactants} n_i\left[\Delta H^0_{f,i} + \bar{c}_{p,i}\left(T_i - T_{ref}\right)\right] - \sum_{products} n_i\left[\Delta H^0_{f,i} + \bar{c}_{p,i}\left(\Xi_{Le}T_{CNAFT} - T_{ref}\right)\right]$$
$$= \begin{cases} 0.207\left(\pi - \pi_{ref}\right) & for\ \left[X_{H_2O}\right]_{reactants} = 0 \\ 0.207\left(\pi - \pi_{ref}\right)\cdot\left(\dfrac{X_{H_2,\ in} + X_{steam,\ in}}{X_{steam,ref}}\right) & for\ \left[X_{H_2O}\right]_{reactants} > 0 \end{cases} \tag{13}$$

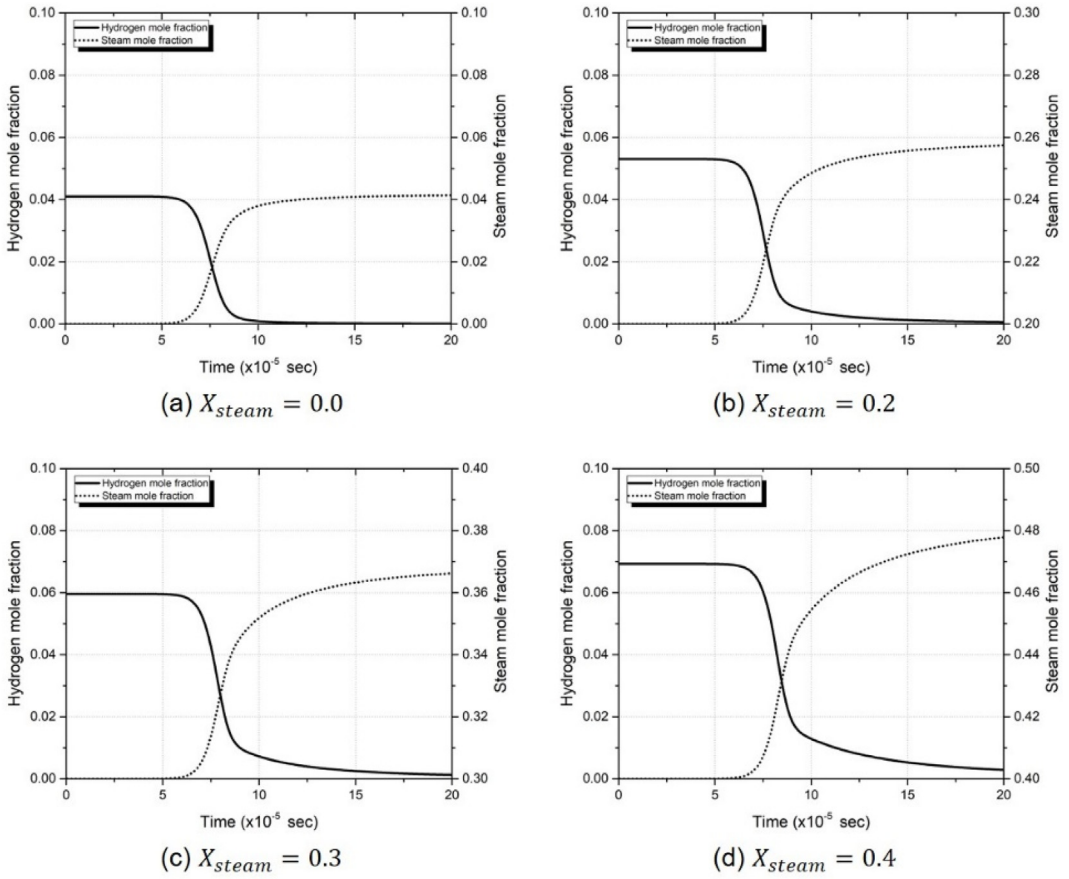

Fig. 9. Temporal evolution of $X_{hydrogen}$, X_{steam} for each limiting H_2-air-steam mixture in a homogeneous adiabatic condition at constant atmospheric pressure and $T_{in} = 1200\,K$ as obtained from numerical integrations with the 7-step mechanism ($X_{steam} = 0.0, 0.2, 0.3, 0.4$).

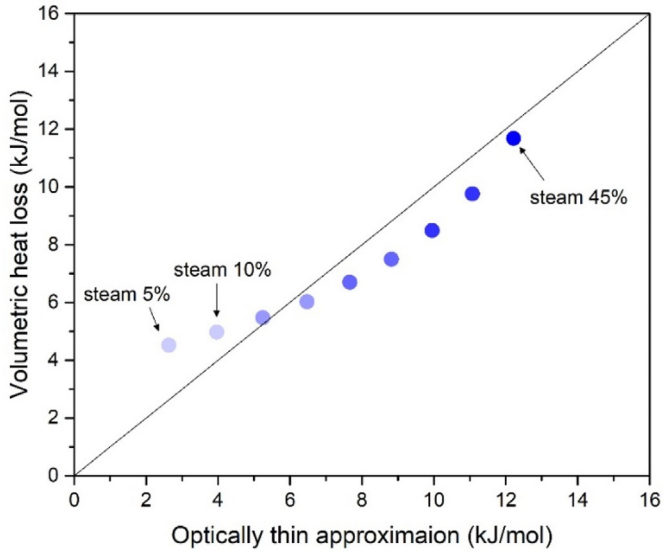

Fig. 10. Accuracy of optically thin approximation according to steam concentration.

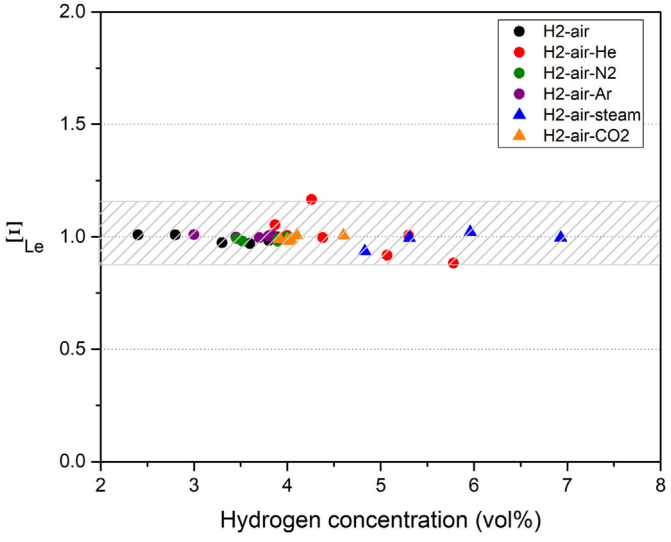

Fig. 11. Calculated Ξ_{Le} values for all referenced experimental results. It was identified that the value did not deviate significantly based on 1.0.

As a result, Fig. 12 shows the improved accuracy of the CNAFT model ($\Xi_{Le} = 1$) by comparing with the experimental results [23–25]. (The MATLAB code for the CNAFT model is available from https://data.mendeley.com/datasets/hgydzjvcch/1)The triangular symbols of H_2-air-steam represent data at steam concentrations of 10, 20, 30, and 40%. Because the FITS experiments have been evaluated as the most sophisticated measurement, the recent MAAP code still relies on its results. The hollow triangle symbols represent the LFL values embedded in the code by correlation form [49]. Although there were slight discrepancies in the interpretation

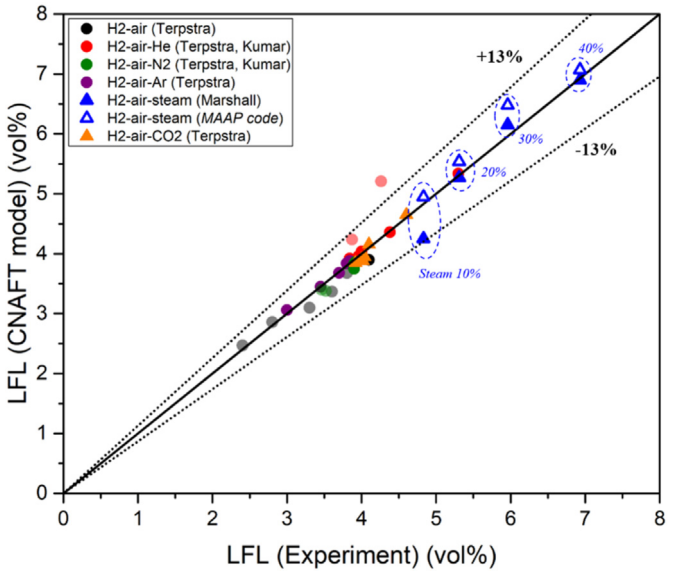

Fig. 12. Validation of the improved CNAFT model with optically thin approximation in various mixture conditions.

of the experimental results, it was noted that the maximum relative error is about 13% even for the H_2-air-steam mixtures, which incorporated severe accident conditions. This reasonable accuracy can also be identified by the CNAFT value at each limiting mixture shown in Table 4. The mixtures exhibit an initial temperature of approximately 400 K under ambient pressure. Although the prediction accuracy for heat loss amount in H_2-air-steam mixtures over 400 K necessitates further investigation, the CNAFT model showed good agreement with Terpstra's and Kumar's experiments for H_2-air mixtures up to 500 K.

In this study, the improved CNAFT model, which can reasonably predict the LFL of hydrogen mixtures, was proposed by considering the indirect radiation mechanism at the flame trailing edge. While previous studies have attempted to predict the LFL through thermal analysis at the stretched flame tip which firstly countering cold unburned gas, this study focused on the extinction process at the nearly unstretched trailing edge. Although the flammability limit model was developed based on the recent observed nature of the hydrogen flame extinction, more detailed analysis of thermal behavior and flow characteristics of flame just before the recirculation flow is our future work. Especially, quantitative evaluation of thermal and fluid properties near the trailing edge can further verify the thermal modeling [32].

The effects of flame instabilities induced by stretched flame front on the CFD simulation and the developed model need to be discussed. The flame instabilities to be issued in deflagration are strongly related to the molecular transport processes [14]. Darrieus-Landau instability (hydrodynamic instability), an intrinsic flame instability in premixed flame, results from the thermal expansion during combustion process. The density difference across the flame imposes perturbations and the flame can no longer propagate at a constant laminar burning velocity. On the other hand, diffusive-thermal instability is important for mixtures with Lewis number lower than unity. The basic principle of diffusive-thermal instability is almost the same as the local burning intensity change by Lewis number magnitude discussed in *Section 2*. The difference between thermal and mass diffusivity in stretched flame intensifies the fluctuation of local burning intensity along the flame front.

The effects of Darrieus-Landau instabilities and diffusive-thermal instabilities were considered in our simulation by the described species transport model with the properties of gases including hydrogen. However, during ultralean flame propagation with normal gravitational condition, the instabilities provide negligible rise of perturbations as discussed by previous researchers [14,16]. The flame mainly propagates upward with overwhelming time scale by buoyancy force. For this reason, evolution of flame surface cracks was not observed in our CFD results even though the concentration approached limit condition. Although the effects of instabilities on flame surface may be captured in more detail at a finer grid size, cellular patterns in near limit hydrogen flames were only observed during downward propagation in Bregeon et al.'s experiments [50]. It implies that the flame instabilities only have non-negligible effect on flame propagation in the absence of large wavelengths such as buoyancy. One of the common ways to analyze the effects of instabilities is to perform flame experiments with microgravity or zero-gravity conditions.

5. Conclusion

In this study, the extinction process of the lean hydrogen flame was investigated by numerical simulation with detailed chemical kinetics. At a hydrogen concentration above the limit, the bubble-like flame with a long flame skirt was observed. When the length is shortened sufficiently by the decrease of the concentration, the recirculation flow was generated during transition from the bubble-like flame to the cap-like flame. The observed primary extinction mechanism can verify the mechanistic thermal approach to predict the LFLs, which was not elaborated sufficiently in previous studies. The CNAFT model with optically thin approximation can reasonably predict the LFL of hydrogen mixtures including H_2O and CO_2 diluent conditions while preserving the advantages of macroscopic flame analysis. We expect that the improved model can provide reliable flammability evaluation and useful insight in industry fields. More detailed analysis of thermal behavior and flow characteristics during extinction process from the bubble flame to cap flame is still needed. Our major findings can be summarized as follows.

1) The generation of recirculating flow causing the weak burning intensity at the flame tip is a major branching point for hydrogen flame extinction. To reach the flame region generating recirculating flow, the length of flame skirt should be short enough by indirect radiation heat loss. In this study, a thermal model for flammability limit was developed based on the primary extinction mechanism.
2) It was confirmed that the total direct radiation heat release rate based on the maximum volumetric rate did not reach 5% of the total direct radiation rate based on the minimum temperature gradient at the trailing edge. The dominant effect of the indirect radiation mechanism for flammability limit was further confirmed by our simulation results.
3) The H_2-air-CO_2 mixtures contain a radiating gas, but there is no difference in heat loss amount from the reference mixture. It seems that the adiabatic condition was approached regardless of the diluent type even radiating gas, below the threshold value of the CNAFT coefficient. On the contrary, the soar of heat loss due to the addition of steam can be predicted by the optically thin approximation.
4) The temporal evolution of hydrogen and steam concentration at reaction zone was investigated by the computing the ignition process in microsecond units. The numerical results verify the assumption that the steam mole fraction at flame front can be

substituted by a complete-combustion approach under lean conditions.

5) The Lewis number effect on the mechanistic model was investigated by introducing a constant factor, Ξ_{Le}. The variation of Ξ_{Le} value according to the mixture type was calculated though the experimental results and it was confirmed that the variation did not reduce the model accuracy significantly.

Declaration of competing interest

The authors declare that they have no known competing financial interests or personal relationships that could have appeared to influence the work reported in this paper.

Acknowledgments

This work was supported by the National Research Foundation of Korea (NRF) and funded by the Ministry of Science, ICT, and Future Planning, Republic of Korea (grant numbers NRF-2016R1A5A1013919 and NRF-2021M2D2A2076382).

References

[1] J. Kim, U. Lee, S.W. Hong, S.B. Kim, H.D. Kim, Spray effect on the behavior of hydrogen during severe accidents by a loss-of-coolant in the APR1400 containment, Int. Commun. Heat Mass 33 (10) (2006) 1207–1216.
[2] A. Bentaib, N. Meynet, A. Bleyer, Overview on hydrogen risk research and development activities: methodology and open issues, Nucl. Eng. Technol. 47 (1) (2015) 26–32.
[3] N.K. Kim, J. Jeon, W. Choi, S.J. Kim, Systematic hydrogen risk analysis of OPR1000 containment before RPV failure under station blackout scenario, Ann. Nucl. Energy 116 (2018) 429–438.
[4] J. Jeon, Y.S. Kim, W. Choi, S.J. Kim, Identification of Hydrogen Flammability in steam generator compartment of OPR1000 using MELCOR and CFX codes, Nucl. Eng. Technol. 51 (2019) 1939–1950.
[5] P. Nikolaidis, A. Poullikkas, A comparative overview of hydrogen production processes, Renew. Sustain. Energy Rev. 67 (2017) 597–611.
[6] J. Jeon, S.J. Kim, Recent progress in hydrogen flammability prediction for the safe energy systems, Energies 13 (23) (2020) 6263.
[7] A.C. Egerton, J. Powling, The limits of flame propagation at atmospheric pressure II. The influence of changes in the physical properties, Proc. Royal Soc. A 193 (1033) (1948) 190–209.
[8] M.G. Zabetakis, Flammability Characteristics of Combustible Gases and Vapors, Bureau of Mines, Washington DC, 1965.
[9] M. Vidal, W. Wong, W. Rogers, M.S. Mannan, Evaluation of lower flammability limits of fuel–air–diluent mixtures using calculated adiabatic flame temperatures, J. Hazard Mater. 130 (1) (2006) 21–27.
[10] G. Shu, B. Long, H. Tian, H. Wei, X. Liang, Flame temperature theory-based model for evaluation of the flammable zones of hydrocarbon-air-CO2 mixtures, J. Hazard Mater. 294 (2015) 137–144.
[11] M. Wu, G. Shu, R. Chen, H. Tian, X. Wang, Y. Wang, A new model based on adiabatic flame temperature for evaluation of the upper flammable limit of alkane-air-CO2 mixtures, J. Hazard Mater. 344 (2018) 450–457.
[12] H.J. Liaw, K.Y. Chen, A model for predicting temperature effect on flammability limits, Fuel 178 (2016) 179–187.
[13] F. Zhao, W.J. Rogers, M.S. Mannan, Calculated flame temperature (CFT) modeling of fuel mixture lower flammability limits, J. Hazard Mater. 174 (1–3) (2010) 416–423.
[14] A.L. Sánchez, F.A. Williams, Recent advances in understanding of flammability characteristics of hydrogen, Prog. Energy Combust. 41 (2014) 1–55.
[15] E. Fernández-Tarrazo, A.L. Sánchez, A. Liñán, F.A. Williams, Flammability conditions for ultra-lean hydrogen premixed combustion based on flame-ball analyses, Int. J. Hydrogen Energy 37 (2) (2012) 1813–1825.
[16] I. Yakovenko, M. Ivanov, A. Kiverin, K. Melnikova, Large-scale flame structures in ultra-lean hydrogen-air mixtures, Int. J. Hydrogen Energy 43 (3) (2018) 1894–1901.
[17] Y. Dong, A.T. Holley, M.G. Andac, F.N. Egolfopoulos, S.G. Davies, P. Middha, H. Wang, Extinction of premixed H_2/air flames: chemical kinetics and molecular diffusion effects, Combust. Flame 142 (4) (2005) 374–387.
[18] J.H. Lee, M. Berman, Hydrogen combustion and its application to nuclear reactor safety, Adv. Heat Tran. 29 (1997) 59–127.
[19] J. Jeon, W. Choi, S.J. Kim, A flammability limit model for hydrogen-air-diluent mixtures based on heat transfer characteristics in flame propagation, Nucl. Eng. Technol. 51 (2019) 1749–1757.
[20] Y.S. Kim, J. Jeon, C.H. Song, S.J. Kim, Improved prediction model for H2/CO combustion risk using a calculated non-adiabatic flame temperature model, Nucl. Eng. Technol. 52 (12) (2020) 2836–2846.
[21] Z. Zhou, Y. Shoshin, F.E. Hernández-Pérez, J.A. van Oijen, L.P. de Goey, Experimental and numerical study of cap-like lean limit flames in H_2-CH_4-air mixtures, Combust. Flame 189 (2018) 212–224.
[22] Z. Zhou, Y. Shoshin, F.E. Hernandez-Perez, J.A. van Oijen, L.P. de Goey, Effect of Lewis number on ball-like lean limit flames, Combust. Flame 188 (2018) 77–89.
[23] M. Terpstra, Flammability Limits of Hydrogen-Diluent Mixtures in Air, MSc thesis, University of Calgary, 2012.
[24] R. Kumar, Flammability limits of hydrogen-oxygen-diluent mixtures, J. Fire Sci. 3 (4) (1985) 245–262.
[25] B.W. Marshall, Hydrogen:air: Steam Flammability Limits and Combustion Characteristics in the FITS Vessel, Sandia National Laboratories, Albuquerque, 1986.
[26] Y. Shoshin, L. Tecce, J. Jarosinski, Experimental and computational study of lean limit methane-air flame propagating upward in a 24 mm diameter tube, Combust. Sci. Technol. 180 (10–11) (2008) 1812–1828.
[27] H. Bordbar, G.C. Fraga, S. Hostikka, An extended weighted-sum-of-gray-gases model to account for all CO_2-H_2O molar fraction ratios in thermal radiation, Int. Commun. Heat Mass 110 (2020), 104400.
[28] G. Krishnamoorthy, A new weighted-sum-of-gray-gases model for CO2–H2O gas mixtures, Int. Commun. Heat Mass 37 (9) (2010) 1182–1186.
[29] J. Jeon, H. Jung, Y.S. Kim, S.J. Kim, Numerical Study of Lean Limit Hydrogen Flames Propagating Upward to Validate a Flammability Limit Model, NURETH-18, Portland, 2019, pp. 4362–4371.
[30] S.R. Turns, An Introduction to Combustion, third ed., McGraw-Hill, New York, 1996, pp. 293–300.
[31] E. Mayer, A theory of flame propagation limits due to heat loss, Combust. Flame 1 (4) (1957) 438–452.
[32] J. Jeon, D. Shin, W. Choi, S.J. Kim, Identification of the extinction mechanism of lean limit hydrogen flames based on recirculation heat transfer, Int. J. Heat Mass Tran. 174 (2021), 121288.
[33] F.E. Hernández-Pérez, B. Oostenrijk, Y. Shoshin, J.A. van Oijen, L.P. de Goey, Formation, prediction and analysis of stationary and stable ball-like flames at ultra-lean and normal-gravity conditions, Combust. Flame 162 (4) (2015) 932–943.
[34] Y. Shoshin, L. De Goey, Experimental study of lean flammability limits of methane/hydrogen/air mixtures in tubes of different diameters, Exp. Therm. Fluid Sci. 34 (3) (2010) 373–380.
[35] V.V. Volodin, V.V. Golub, A.D. Kiverin, K.S. Melnikova, A.Y. Mikushkin, I.S. Yakovenko, Large-scale dynamics of ultra-lean hydrogen-air flame kernels in terrestrial gravity conditions, Combust. Sci. Technol. 193 (2) (2021) 225–234.
[36] Y. Shoshin, J. Jarosinski, On extinction mechanism of lean limit methane–air flame in a standard flammability tube, Proc. Combust. Inst. 32 (1) (2009) 1043–1050.
[37] J. Jarosinski, R. Strehlow, A. Azarbarzin, The mechanisms of lean limit extinguishment of an upward and downward propagating flame in a standard flammability tube, Symp. (Int.) Combust. 19 (1) (1982) 1549–1557.
[38] Y. Ju, H. Guo, K. Maruta, F. Liu, On the extinction limit and flammability limit of non-adiabatic stretched methane–air premixed flames, J. Fluid Mech. 342 (1997) 315–334.
[39] A.R. Tajik, P. Kuntikana, S.V. Prabhu, V. Hindasageri, Effect of preheated mixture on heat transfer characteristics of impinging methane–air premixed flame jet, Int. J. Heat Mass Tran. 86 (2015) 550–562.
[40] Z. Wei, C. Leung, C. Cheung, Z. Huang, Effects of H2 and CO2 addition on the heat transfer characteristics of laminar premixed biogas–hydrogen Bunsen flame, Int. J. Heat Mass Tran. 98 (2016) 359–366.
[41] H.F. Coward, G.W. Jones, Limits of Flammability of Gases and Vapors, Bureau of Mines, Washington DC, 1952.
[42] C. Law, F. Egolfopoulos, A unified chain-thermal theory of fundamental flammability limits, Symp. (Int.) Combust. 24 (1) (1992) 137–144.
[43] K. Lakshmisha, P. Paul, H. Mukunda, On the flammability limit and heat loss in flames with detailed chemistry, Symp. (Int.) Combust. 23 (1) (1991) 433–440.
[44] V.J. Mascarenhas, C.N. Weber, P.R. Westmoreland, Estimating flammability limits through predicting non-adiabatic laminar flame properties, Proc. Combust. Inst. 38 (2021) 4673–4681.
[45] S. Zheng, R. Sui, Y. Yang, Y. Sun, H. Zhou, Q. Lu, An improved full-spectrum correlated-k-distribution model for non-gray radiative heat transfer in combustion gas mixtures, Int. Commun. Heat Mass 114 (2020), 104566.
[46] R. Seigel, J.R. Howell, Thermal Radiation Heat Transfer, McGraw-Hil, New York, 1981, p. 836.
[47] A.L. Sánchez, E. Fernández-Tarrazo, P. Boivin, A. Liñán, F.A. Williams, Ignition time of hydrogen–air diffusion flames, Compt. Rendus Mec. 340 (2012) 882–893.
[48] D. Fernández-Galisteo, A. Sánchez, A. Liñán, F. Williams, The hydrogen–air burning rate near the lean flammability limit, Combust. Theor. Model. 13 (4) (2009) 741–761.
[49] M.G. Plys, Hydrogen production and combustion in severe reactor accidents: an integral assessment perspective, Nucl. Technol. 101 (1993) 400–410.
[50] B. Bregeon, A.S. Gordon, F.A. Williams, Near-limit downward propagation of hydrogen and methane flames in oxygen nitrogen mixtures, Combust. Flame 33 (1978) 33–45.